Section 2

Data sets, diagnostic and dynamical investigations, statistical post-processing , multi-year reanalyses and associated studies

Moisture transport across south eastern Australia using stable isotopes in precipitation

Vaughan Barras[1], Ian Simmonds[1], David Etheridge[2]

[1] School of Earth Sciences, The University of Melbourne, Victoria, Australia, 3010
[2] CSIRO Atmospheric Research, Aspendale, Victoria, Australia, 3195
Email: vbarras@earthsci.unimelb.edu.au

The relative abundances of the stable isotopes ^{18}O and ^{2}H in precipitation can reveal information about the condensation history of atmospheric moisture. Stable isotopes allow the diagnosis of atmospheric circulation (Lawrence et al., 1982), moisture source regions and atmospheric transport (Rindsberger et al., 1990). Investigation of precipitation records over south eastern Australia is being approached in two ways. Firstly, with the establishment of the Melbourne University Network of Isotopes in Precipitation (MUNIP). This is a series of collection sites across the Melbourne metropolitan region with the aim of sampling rain half hourly during particular rain events to document isotopic variability over small scales in time and space. The first full observational experiment occurred on June 9, 2004. Initial analysis of the atmospheric circulation around the hemisphere for this rain event has been performed using NCEP2 reanalysis data (Kanamitsu et al., 2002). From these fields it has been possible to reconstruct three dimensional backward trajectories for air parcels arriving at Melbourne at a number of different levels in the lower troposphere. The scheme described by Noone (2001) estimates the gridded wind field using a fourth order Runge-Kutta finite difference with the Lagrangian pathway approximated by applying the law of cosines on a sphere. The resulting six day backward trajectories (Figure 1a) show the convergence of low, relatively dry air with more moist upper level air as they pass towards south eastern Australia. The gradual uplift of the upper level parcels in the 24 hours preceding the rain event (Figure 1b) is associated with cloud formation and the majority of the fractionation of the air mass.

The second approach to this investigation is through simulation of events and experimentation using the Melbourne University General Circulation Model (MUGCM). The model is a development of that described by Simmonds (1985) with nine vertical levels and includes an isotopic fractionation module as described by Noone and Simmonds (2002). The MUNIP analyses provide an important basis for evaluating the moisture parametrisations within MUGCM with testing phases continuing.

Kanamitsu M., Ebisuzaki W., Woolen J., Yank S-K., Hnilo JJ., Fiorino M., Potter GL., NCEP-DOE AMIP II Reanalysis (R2), *Bull. Amer. Met. Soc., 83*, 1641-1643, 2002.

Lawrence J.R., Gedzelman S.D., White J.W.C., Smiley D., Lazov P., Storm trajectories in eastern US D/H isotopic composition of precipitation, *Nature, 296*, 638-640, 1982.

Noone D., A physical assessment of variability and climate signals in Antarctic precipitation and the stable isotope record, PhD thesis, University of Melbourne, Melbourne, 2001.

Noone D., Simmonds I., Associations between $\delta^{18}O$ of water and climate parameters in a simulation of atmospheric circulation for 1979-95, *Journ. Clim., 15*, 3150-3169, 2002.

Rindsberger M., Jaffe S., Rahamim S., Gat J.R., Patterns of the isotopic composition of precipitation in time and space: data from the Israeli storm water collection program., *Tellus, 42B*, 263-271, 1990.

Simmonds I, Analysis of the spinup of a General Circulation Model, *Journ. Geophys. Res., 90*, 5637-5660, 1985.

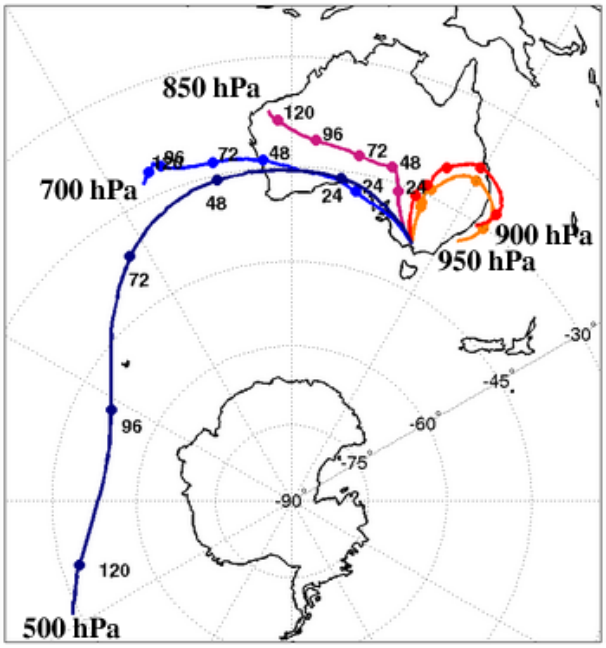

(a)

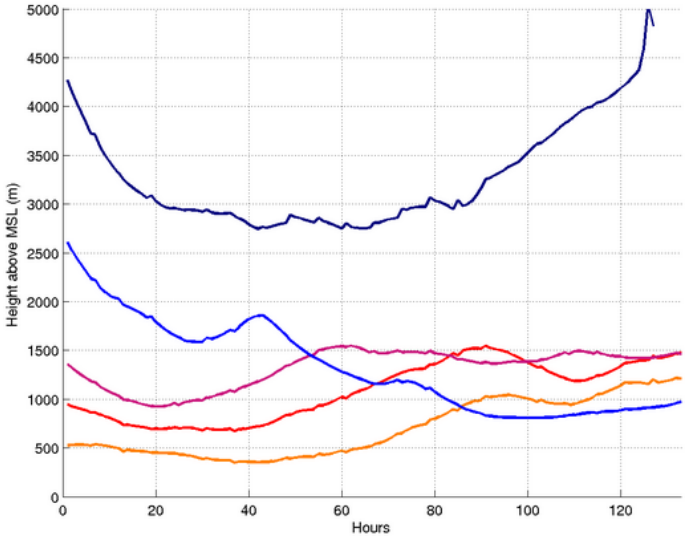

(b)

Figure 1: (a) 6 day backward trajectories for 9/6/2004 rain event in Melbourne. Trajectories released at 950, 900, 850, 700, 500hPa levels with markers indicating parcel position at 24 hourly intervals. (b) Parcel trajectory levels in metres above surface. Abscissa values are backwards in time from parcel launch at $x = 0$

Links between the Southern Annular Mode and Australian rainfall

Belinda Meneghini[1], Ian Simmonds[1] and Ian N. Smith[2]

[1]School of Earth Sciences
The University of Melbourne
Victoria, 3010, Australia

[2]CSIRO Atmospheric Research
Private Mail Bag No. 1, Mordialloc
Victoria, 3195, Australia

The Southern Annular Mode (SAM) is an out-of-phase fluctuation in pressure at the mid- and high-latitudes of the Southern Hemisphere (SH). The dynamics (and the involvement of transient eddies) is still far from understood (Rashid and Simmonds, 2004, 2005). An index of the SAM (the AOI) can be taken as the normalized zonal average pressure difference between 40^{o} and 65^{o}S (Gong and Wang, 1999). The index shows strong positive trend since the mid-1970s. Over that time there have been significant decreases in winter rainfall in southwest Western Australia, Victoria and Tasmania (Smith, 2004). Given the role of the transient eddies in maintaining the SAM (and the trends that SH cyclones have displayed over that period (Simmonds and Keay, 2000)), we are exploring the extent to which these Australian rainfall changes can be seen as associated with the SAM.

Over the period 1958 – 2002 we extract the Australian monthly rainfall (Bureau of Meteorology) and also calculate the AOI from the NCEP reanalysis. Fig. 1 shows the correlation of the July time series. Significant (95% confidence level) negative correlations are found in the southeast and southwest corners of the continent. A belt of significant *positive* correlations over a large portion of NSW, extending to the west. This overall structure is strongly suggestive of the meridional translation of rain-bearing systems according to the phase of the SAM.

Many authors (e.g., Simmonds and King (2004)) have emphasised that the SAM is far from zonally symmetric, and clearly *local* reflections of the SAM are associated with regional climate variations. To explore this we have derived an *Australian region* AOI which follows the above definition, but makes use of the data only in the 90-180^{o}E sector. The pattern of correlations with this index resemble those above, though the negative correlations referred to above are considerably stronger.

Gong, D. Y., and S. W. Wang, 1999: Definition of Antarctic Oscillation Index. *Geophysical Research Letters,* **26,** 459-462.

Rashid, H. A., and I. Simmonds, 2004: Eddy-zonal flow interactions associated with the Southern Hemisphere annular mode: Results from NCEP-DOE reanalysis and a quasi-linear model. *Journal of the Atmospheric Sciences*, **61,** 873-888.

Rashid, H. A., and I. Simmonds, 2005: Southern Hemisphere annular mode variability and the role of optimal nonmodal growth. *Journal of the Atmospheric Sciences,* (in press).

Simmonds, I., and K. Keay, 2000: Variability of Southern Hemisphere extratropical cyclone behavior 1958-97. *Journal of Climate,* **13,** 550-561.

Simmonds, I., and J. C. King, 2004: Global and hemispheric climate variations affecting the Southern Ocean. *Antarctic Science,* **16,** 401-413.

Smith, I., 2004: An assessment of recent trends in Australian rainfall. *Australian Meteorological Magazine,* **53,** 163-173.

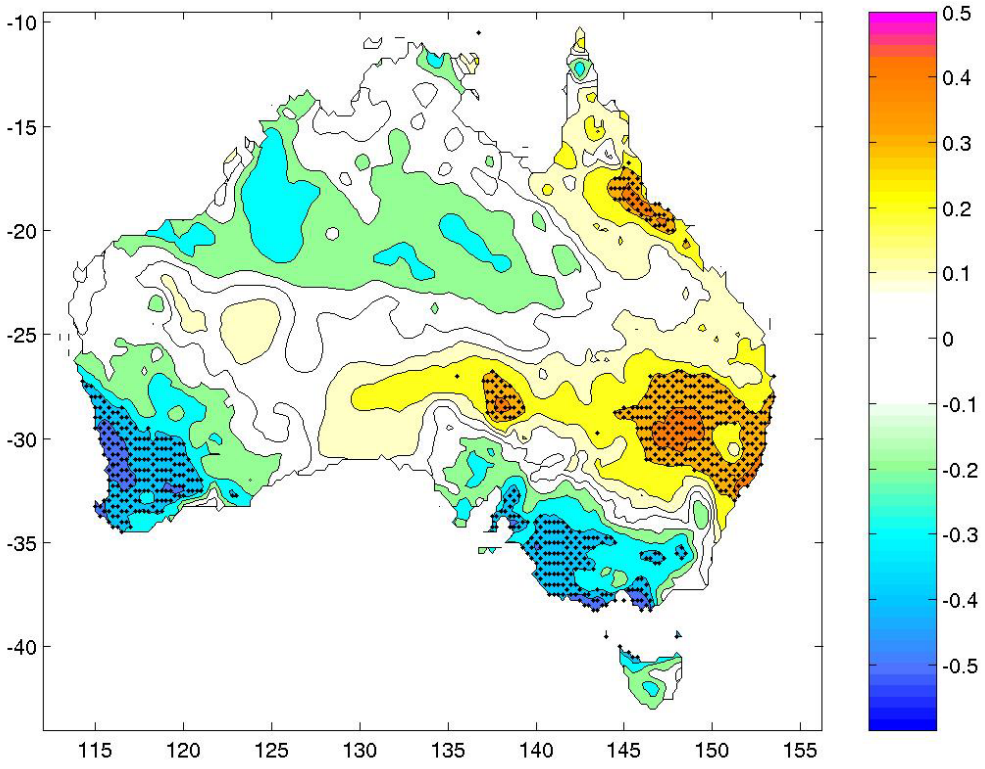

Figure 1: Correlation of July AOI and precipitation (1958 – 2002) (contour interval is 0.1). Stippling denotes regions over which the correlations differ significantly from zero (95% confidence level).

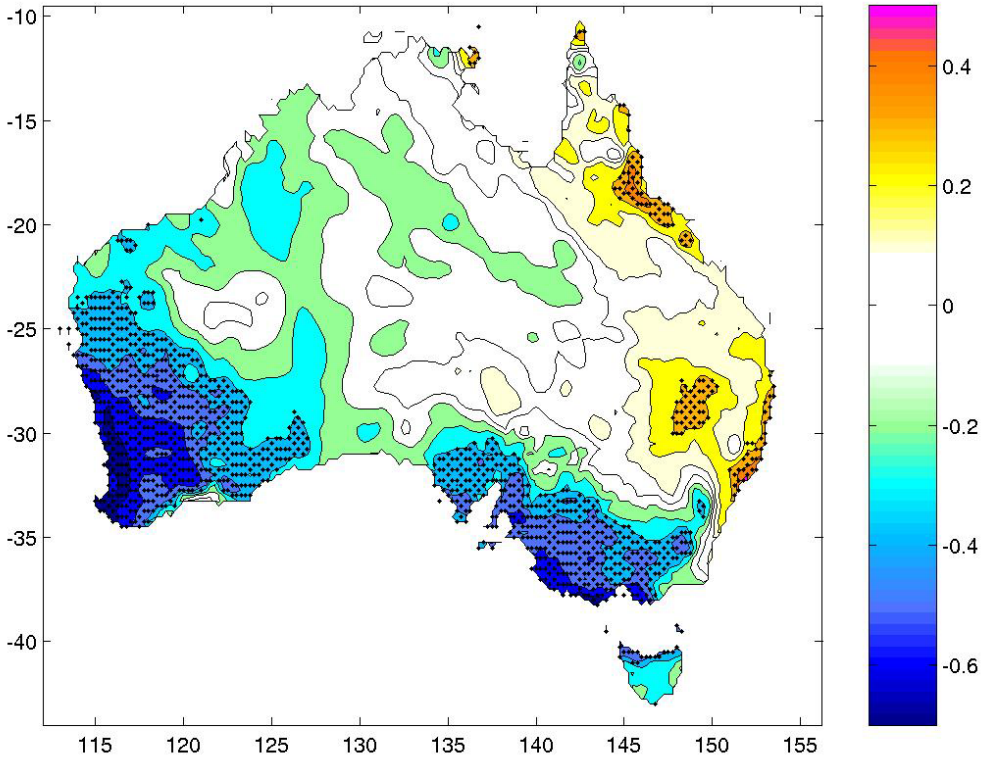

Figure 2: As for Fig. 1, but AOI calculated from data in the 90-180^{o}E sector only.

On the structure of the eye of hurricane Isabel.

Pokhil A.E.,
Russian Hydrometeorological Research Center, 9-11, Big
Predtechensky lane, 123242, Moscow, Russia, pokhil@mecom.ru

Tropical cyclones (TC) belong to the most destructive natural phenomena and represent a danger for almost 50 countries throughout the world. The TC landfalls involve victims among the population and cause significant damage to the economy. At the same time, a TC's making no landfall in the Russian Far East led to prolonged absence of fresh water in the whole region. The forecast of the motion and evolution of TCs strongly depends on gaining insight into the processes that take place in a TC.

Isabel, one of the strongest superhurricanes has been studied. It crossed the Atlantic from September to October 2003 and reached the stage of a hurricane with the pressure 915 hPa and the wind velocity 170 knots. The hurricane proceeded to the state North Carolina, crossed the states Virginia, West Virginia, Pennsylvania and, after turning into an extratropical cyclone, proceeded to the Great Lakes and further to Canada. Its path exceeded 5.500 km.

When observing the motion of TC Isabel, on the photographs taken from the satellite GOES-12 East (G-12) unusual structures were detected in the eye of the hurricane in the microwave range. These structures form near the hurricane eye wall, where huge velocity gradients and strong turbulence take place, and upward and downward fluxes occur. The velocity fluctuations reach here tremendous values.

The eye looked as a circle split into five sectors, with an oval vortex formation in every one, which occupied the largest part of the sector. At the moment of observations the diameter of the eye was 35 - 40 km, the diameters of each of the vortices constituted 10 – 12 km. One observed cyclonic rotation of this system formed of five cyclonic vortices round the TC center. The performed estimation has demonstrated that the mean linear velocity of the relative rotation was about 115 – 140 km/h.

The system of vortices gradually transformed, one of the five vortices began to attract and capture the neighboring left vortex; as a result a system of four vortices rotating round the center formed. Further rather complex deformations of the vortices

took place (pushing apart, contraction, capturing of one vortex by another); the resulting pattern comprised three stretched vortices.

To get insight into the behavior of the vortices in the TC, numerical experiments using a barotropic model /1, 2/ with several interacting perfect vortices were helpful. The comparison of the rotation and transformation of the vortices observed in the eye of hurricane Isabel with the results obtained using the numerical model (Fig.2) demonstrates the identical character of the behavior of the vortices in the eye of the real TC and those simulated by the barotropic model.

References

1. A.E.Pokhil, Some prerequisites for generation of a large vortex and characteristics of vortex interaction. – Meteorology and Hydrology, 1996, no.2, pp. 24 – 32.

2. A.E.Pokhil and I.V.Polyakova, Interaction of cyclonic vortex pair in a barotropic atmospheric model, Meteorology and Hydrology, 1992, no.2, pp. 40 – 50.

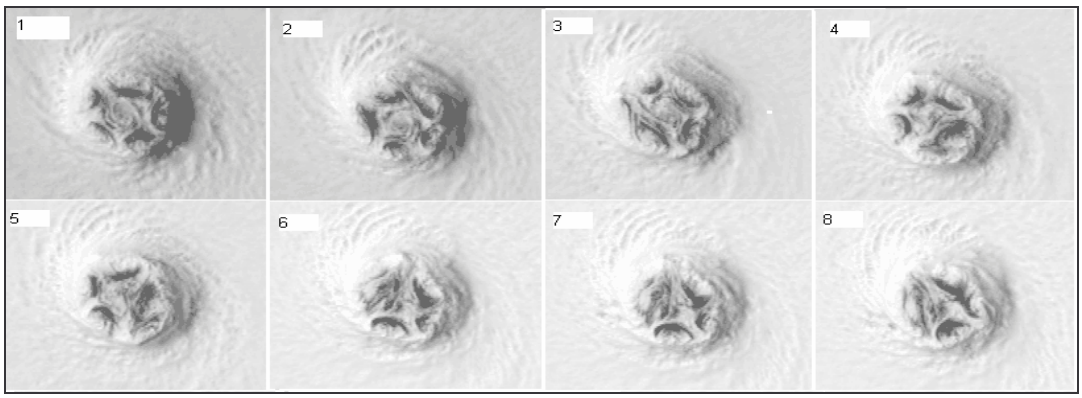

Figures 1. Evolution of the vortices in the eye of hurricane Isabel.

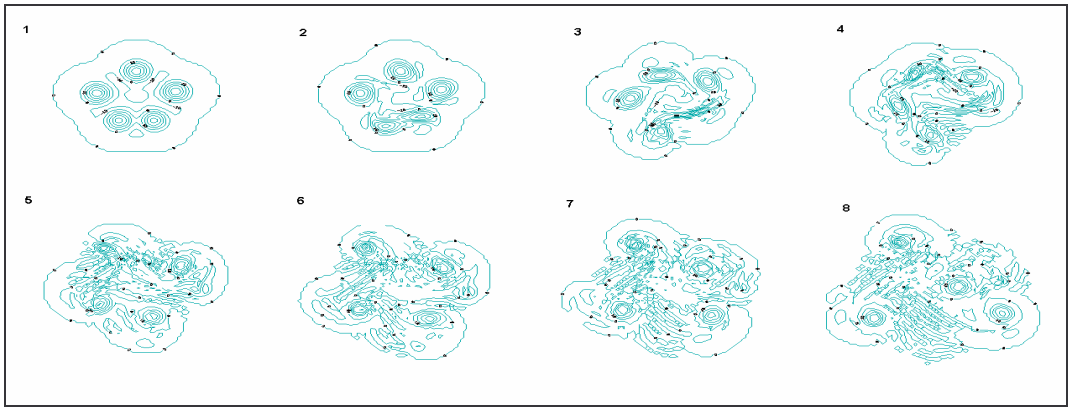

Figures 2. Evolution of the vortices simulated using the barotropic model.

The WGNE Intercomparison of Tropical Cyclone Track Forecasts by Operational Global Models

Ryota SAKAI, Munehiko YAMAGUCHI
Numerical Prediction Division, Japan Meteorological Agency
(E-mail: ryouta.sakai-a@met.kishou.go.jp, m-yamaguchi@met.kishou.go.jp)

1. Introduction

WGNE has conducted an intercomparison of Tropical Cyclone (TC) track forecasts by operational global models since 1991(Tsuyuki et al. 2002). JMA collects forecast data from participating NWP centers, verifies TC track forecasts and reports the verification results at the WGNE meeting every year. At the beginning of this intercomparison, the verification was carried out only for the western-North Pacific region with three NWP centers; JMA[1], ECMWF[2], UKMO[3]. At present, the verification area is expanded to all regions where TCs are analyzed under the WMO Tropical Cyclone Programme. CMC[4], DWD[5], BoM[6] and NCEP[7] have participated since 1994, 2000, 2003, 2003, respectively.

In this paper, the verification results for the western-North Pacific region, the eastern-North Pacific region, the North Atlantic region and the Southern Hemisphere region are shown.

2. Dataset and method

Analyzed TC position data (besttrack) distributed by various organizations (Table 1) are used in this verification. Table 2 shows the specification of dataset provided by participating NWP centers. The TC position error is defined as an absolute distance between a predicted TC position and the besttrack. The predicted TC position is detected from the mean sea level pressure (MSLP) of prediction at 12 hour intervals. Each position is the nearest point from a “guess” point among minimum MSLP points within 500 km from the guess point. The guess point for each forecast time is decided as follows:

(1) Initial time: Besttrack position.
(2) FT+12: The initial TC position.
(3) FT+24 or later: A linearly extrapolated position by the last 2 forecast positions.

In case there are no minimum MSLP points satisfying above condition, tracking is terminated. The verification is carried out for the TCs analyzed in the besttrack.

3. Western-North Pacific region

The time series of position error for 72 hour forecast from 1991 to 2003 is shown in Figure 1(a). In this verification, the samples which all NWP centers can track are selected. Although there is an interannual variation, significant improvement is seen in all NWP centers. Figure 1(b) indicates the position error in 2003. The minimum position error in all NWP centers is approximately 120, 220, 320 km at 24, 48, 72 hour forecast, respectively. The NWP centers which have adopted TC bogus technique (i.e. JMA, UKMO and NCEP) have smaller position error at all forecast times. Although ECMWF doesn’t adopted TC bogus technique, its position error is relatively small after 12 hour forecast. This result shows that ECMWF produces initial fields of high quality for TC forecast without TC bogus technique.

Figure 2 shows the scattering diagram of position error for 72 hour forecast. The Y-axis represents position error of Along Track (AT) direction and the X-axis does Cross Track (CT) direction. According to the direction of TC movement estimated by predicted TC positions, the plotted marks are classified into three categories, “Before Recurvature” (red), “During Recurvature” (green) and “After Recurvature” (blue). The two systematic errors are seen in almost all NWP centers. One is CT direction’s positive error in “Before” stage. As TCs move toward west in “Before” stage, this error indicates northward bias against analyzed TC position. The other is a large spread of AT direction’s error in “After” stage. This shows that error concerned with TC speed forecast is dominant in “After” stage.

4. Eastern-North Pacific, North Atlantic and Southern Hemisphere regions

Figures 3, 4 and 5 show the verification results for the eastern-North Pacific, the North Atlantic and the Southern Hemisphere regions, respectively. Since the number of samples are not enough for significant statistics, the samples which each NWP center can track are selected for its verification and the result of the eastern-North Pacific region is shown up to 72 hour forecast. The position error of UKMO and NCEP, which have adopted TC bogus technique, is smaller than that of the other NWP centers at initial time. After 24 hour forecast, however, there is no noticeable difference between the position error of the NWP centers with TC bogus and that of the NWP centers without TC bogus.

Reference

Tsuyuki, T. et al., 2002: The WGNE intercomparison of typhoon track forecasts from operational global models for 1991-200. WMO-BULLETIN, vol.5, No.3, 253-257.

---

[1]Japan Meteorological Agency, [2]European Centre for Medium-range Weather Forecasts, [3]United Kingdom Meteorological Office,
[4]Canadian Meteorological Centre, [5]Deutscher Wetterdienst, [6]Australian Bureau of Meteorology, [7]National Centers for Environment Prediction

Table 1 Specification of verification data provided by NWP centers

NWP center	Since	Horizontal Resolution of Provided Data [degree]	TC bogus
JMA	1991	2.5 x 2.5 (1991-1995), 1.25 x 1.25 (1996-2003)	Use (Only the western-North Pacific region)
ECMWF	1991	2.5 x 2.5 (1991-1997), 1.0 x 1.0(1998), 0.5 x 0.5 (1999-2002)	No
UKMO	1991	2.5 x 2.5 (1991-1996), 0.83 x 1.25 (1997), 1.25 x 1.25 (1998-2001), 0.83 x 0.56 (2002-2003)	Use
CMC	1994	1.0 x 1.0 (1994-2003)	No (1995-1999: Use around the North America)
DWD	2000	0.75 x 0.75 (2000-2003)	No
BoM	2003	1.0 x 1.0 (2003)	No
NCEP	2003	0.75 x 0.75 (2003)	Use

Table 2 Besttrack Data

Region	Data Source
western-North Pacific	RSMC-Tokyo
eastern-North Pacific	RSMC-Miami
Central Pacific	RSMC-Honolulu
North Atlantic	RSMC-Miami
North Indian	JTWC
Southern Hemsophere	JTWC

RSMC: Regional Specialized Meteorological Centre
JTWC: Joint Typhoon Warning Center

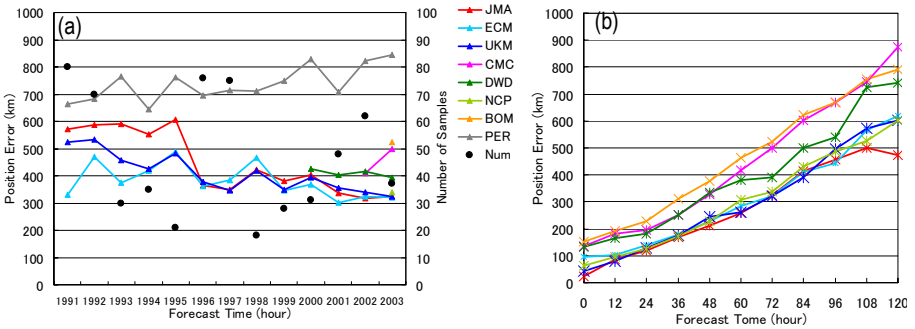

Fig. 1(a) Time series of position error for 72 hour forecast in the western-North Pacific region (1991-2003).
PER: Persistency forecast, Num: Number of samples, JMA: JMA, ECM: ECMWF, UKM: UKMO, CMC, CMC, DWD: DWD, NCP: NCEP, BOM: BoM. (b) Position error in western-North Pacific region in 2003.

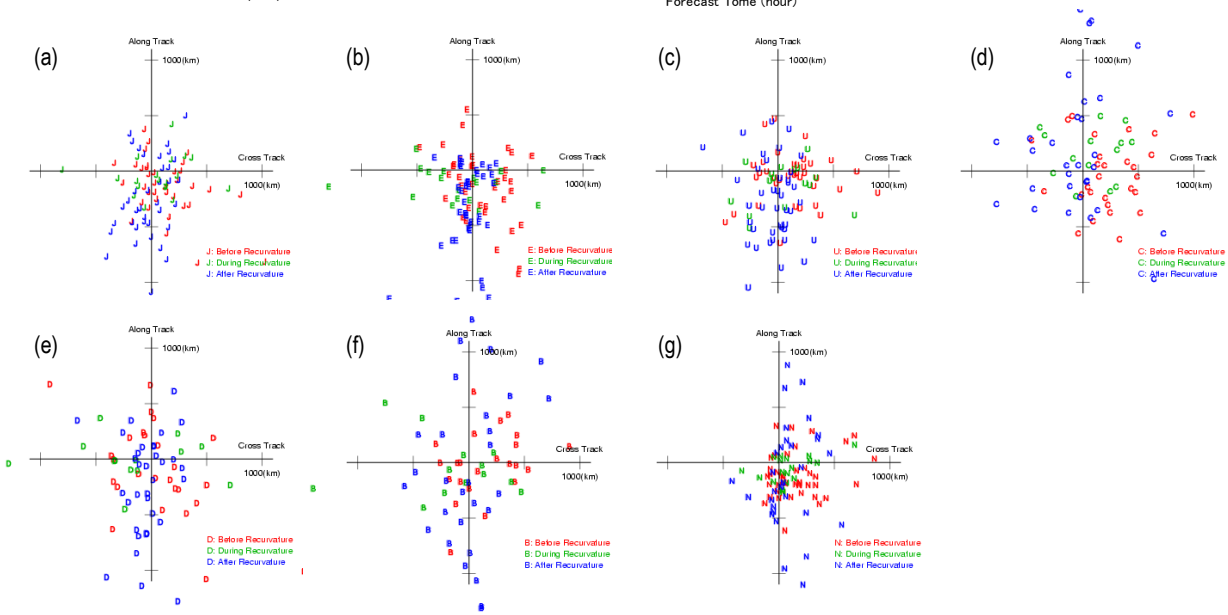

Fig. 2 Scattering diagram of TC positions at 72 hour forecast in 2003. (a) JMA, (b) ECMWF, (c) UKMO, (d) CMC, (e) DWD, (f) BoM, (g) NCEP. Red mark: Before recurvature, Green mark: During recurvature, Blue mark: After recurvature.
Each mark means a relative forecast TC position as seen from the besttrack (the origin). Y-axis represents position errors in Along Track (AT) direction and X-axis does that in Cross Track (CT) direction. Unit: km.

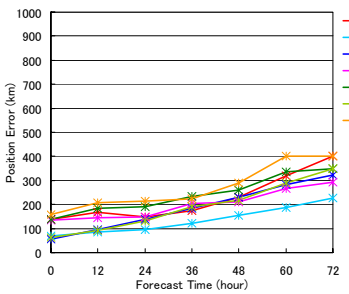

Fig. 3 Position error in the eastern-North Pacific region in 2003. Legend is the same as Fig. 1.

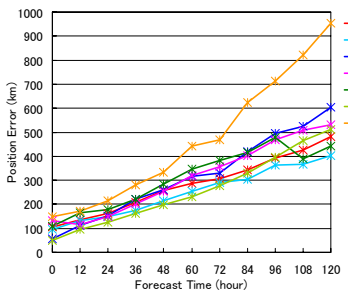

Fig. 4 Position error in the North Atlantic region in 2003. Legend is the same as Fig. 1.

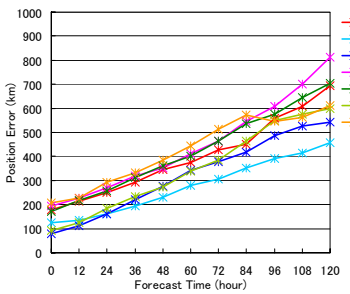

Fig. 5 As in Fig.4 but for the Southern Hemisphere region.

Verification of Quantitative Precipitation Forecasts over Japan from the Operational Numerical Weather Prediction Models (WGNE precipitation forecast intercomparison project)

Takuya Sakashita, Masayuki Hirai
Numerical Prediction Division, Japan Meteorological Agency
(E-mail: sakashita@met.kishou.go.jp, m-hirai@met.kishou.go.jp)

1. Introduction

The Japan Meteorological Agency (JMA) has verified quantitative precipitation forecasts (QPFs) from operational NWP models over Japan in the framework of the WGNE precipitation forecast intercomparison project. A number of reports on this project have already appeared (e.g., Ebert et al. 2003). Hirai and Sakashita (2004) reported the findings on the verification results before September 2003 over Japan. This paper reports the results of the verification up to September 2004.

2. Verification methods

Table 1 indicates the specifications of the QPFs data sent by each NWP centers as of September 2004. A fine resolution data from DWD becomes available this year. The verification methods and other specifications of the data are the same as Hirai and Sakashita (2004). Both the observational data from the rain gauge network and QPFs are upscaled by averaging or downscaled by interpolation to a verification grid of 80km mesh on polar stereo projection.

3. Verification results

(1) 24-h QPFs Verification Results

Figure 1 shows the time series of frequency bias score (BS) and equitable threat score (ETS) of 24h-accumulated precipitation for 3-day forecasts (FT=48-72h) over Japan. ETS for most models tends to have seasonal variations: high ETS in winter and low ETS in summer. It is also found that BS shows a seasonal difference for some models. The similar features of ETS are reported by the verification in the United States, Germany and southwestern Australia (Ebert et al. 2003).

Figure 2 shows BS and ETS for 3-day forecasts (FT=48-72h) with respect to precipitation thresholds in the summer of 2004. Most models tend to overestimate the frequency of light precipitation, as in the summer of 2003 (Hirai and Sakashita 2004).

(2) 6-h QPFs Verification Results

Figure 3 shows BS and ETS for 6-h forecasts in the summer of 2004. It is found that BS for each model is larger in daytime (from 09 to 15 o'clock in Japan standard time) than nighttime and that BS at the beginning of forecast (FT=00-06h) is especially high for some models (e.g., UKMO and JMA). Similar results are seen in the summer of 2003 (Hirai and Sakashita 2004). The features described above are not so significant in winter for all models (not shown).

References

Ebert, E. E., U. Damrath, W. Wergen and M. E.Baldwin, 2003: The WGNE assessment of Short-term Quantitative Precipitation Forecasts. Bull. Am. Meteorol. Soc., **84**, 481-492.

M. Hirai and T. Sakashita, 2004: Verification of Quantitative Precipitation Forecast from Operational Numerical Weather Prediction Models over Japan. *CAS/JSC WGNE Research Activities in Atmospheric and Oceanic Modelling*, **34**, 0601-0602.

Table 1. The specifications of the QPFs data sent by NWP centers as of September 2004.

NWP center	horizontal resolution of data(deg.)	forecast time (h)	verified since	
ABoM	1.25×1.25	12,24,36,…,120	Aug 2002	*1
DWD	0.50×0.50	6,12,18,…,72	Jul 2002	*2
ECMWF	0.50×0.50	6,12,18,…,72	Apr 2002	*3
NCEP	1.00×1.00	6,12,18,…,72	Aug 2002	*4
UKMO	0.83×0.56	6,12,18,…,96	Oct 2001	*5
JMA	0.56×0.56	3,6,9,12,…,72	Apr 2002	*6

*1: Australian Bureau of Meteorology
*2: Deutscher Wetterdienst
24-h accumulated QPFs data received before Sep 2002.
*3: European Centre for Medium-Range Weather Forecasts
*4: National Centers for Environment Prediction
(Aviation model)
*5: United Kingdom Meteorological Office
12-h accumulated QPFs data received before Sep 2002.
*6: Japan Meteorological Agency

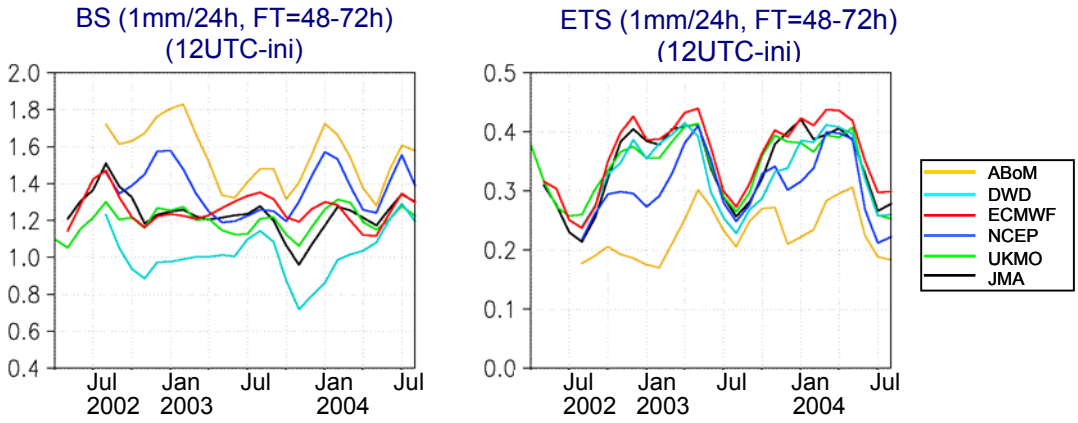

Fig. 1. Monthly time series of BS (left) and ETS (right) of 24-h precipitation for 3-day forecasts (FT=48-72h) from April 2002 to August 2004. The threshold is 1[mm/24h]. Scores are calculated for three consecutive months (from the previous month to the next month).

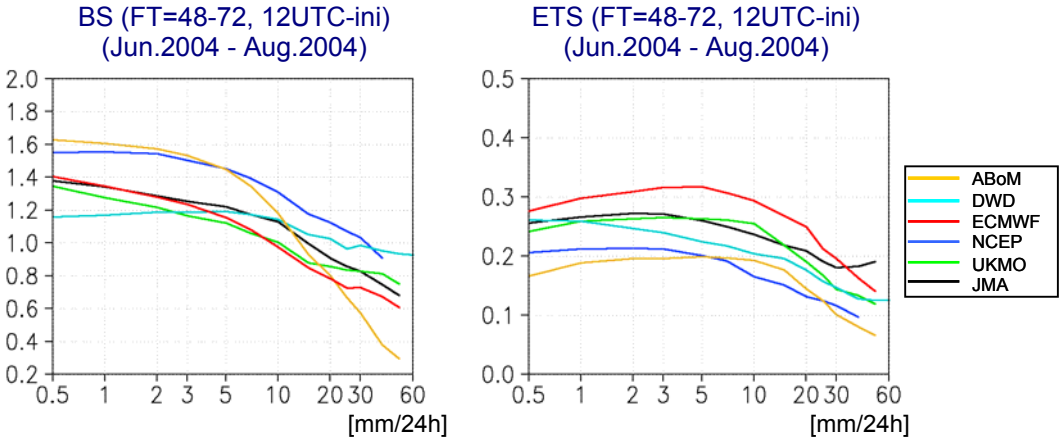

Fig. 2. BS (left) and ETS (right) with respect to precipitation threshold of 24-h precipitation for 3-day forecasts (FT=48-72h) from June 2004 to August 2004. Initial time for each model is 12 UTC. The score is not plotted when the number of events in either observation or forecast is less than 450.

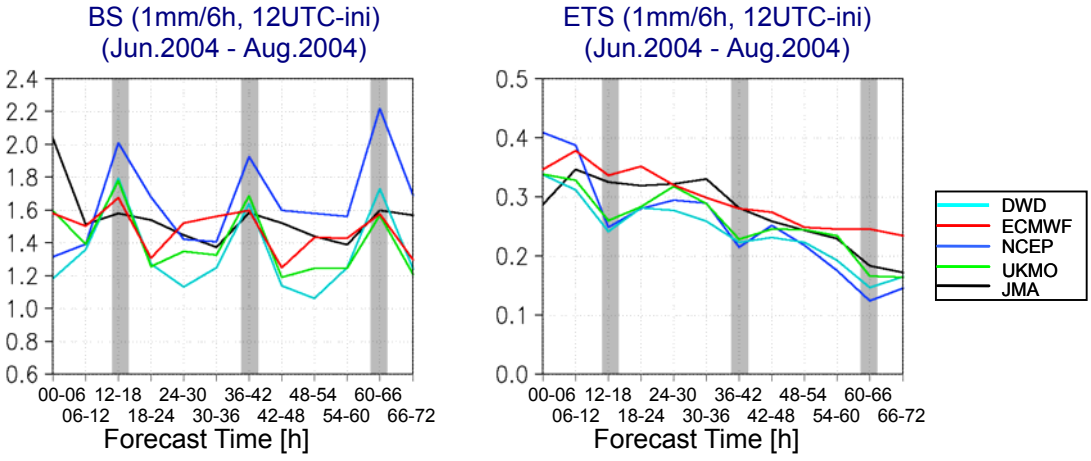

Fig. 3. BS (left) and ETS (right) from June 2004 to August 2004 with respect to forecast time. Precipitation threshold is 1[mm/6h]. The shaded area indicates daytime in Japan (from 09 to 15 o'clock in Japan standard time).

Antarctic sea ice variability and high-latitude fluxes

Ian Simmonds[1], Anthony Rafter[1] and Andrew B. Watkins[2]

[1]School of Earth Sciences
The University of Melbourne
Victoria, 3010, Australia

[2]National Climate Centre
Bureau of Meteorology
GPO Box 1289K, Melbourne
Victoria, 3001, Australia

The Antarctic sea ice region has long been known to exert considerable influence on weather and climate in the high southern latitudes. One of the reasons for this influence is that the presence of sea ice dramatically impacts on the interaction between the atmosphere and surface, and particularly on the surface fluxes of momentum, moisture, and latent and sensible heat. These effects, in turn, influence the boundary layers in both the atmosphere and ocean. The area covered by Antarctic sea ice varies seasonally from a minimum of about 4×10^6 km^2 in February to a maximum of 19×10^6 km^2 in September this dramatic seasonality significantly modulates the nature of the interactions. Our group has an ongoing program exploring these interactions, particularly in the marginal ice zones (e.g., Watkins and Simmonds 1998, Simmonds 2003, White *et al.* 2004, Simmonds *et al.* 2005).

To undertake this analysis and modelling work we make use of the most recent SMMR (years 1978-1987) and SSM/I (1987-2000) GSFC Antarctic sea ice data set (Cavalieri *et al*. 1999). We here show the variability of the sea ice edge (defined to be the location of the 15% concentration contour (Parkinson 2004)). Figure 1 shows the longitudinal structure of the mean edge in December, March, June and September. There is a significant seasonal cycle, at virtually all longitudes, and hence the nature of the interaction of the atmospheric boundary layer and the surface will change dramatically over the course of the year.

Sea ice coverage also undergoes considerable interannual variability which, again, has considerable implications for exchanges across the boundary. To quantify this variability the Figure 2 shows the configuration of the maximum and minimum sea ice extents observed in the record for the four key months, along with the interannual standard deviations about the mean. In December significant variability is apparent in the western hemisphere and off Queen Maud Land. The edge retreats back almost to the Antarctic coast in March over most of the eastern hemisphere and hence little variability is displayed there, while significant variability is seen to the east of the Ross Sea and in the Weddell Sea. During the ice growth phase (e.g., June and September) there tends to be more longitudinal symmetry in the variability, with temporal standard deviations of typically 1 degree (111 km) or more.

Cavalieri, D. J., C. L. Parkinson, P. Gloersen, J. C. Comiso and H. J. Zwally, 1999: Deriving long-term time series of sea ice cover from satellite passive-microwave multisensor data sets. *J. Geophys. Res.,* **104,** 15803-15814.

Parkinson, C. L., 2004: Southern Ocean sea ice and its wider linkages: Insights revealed from models and observations. *Antarc. Sci.,* (in press).

Simmonds, I., 2003: Regional and large-scale influences on Antarctic Peninsula climate. *Antarctic Peninsula Climate Variability: A Historical and Paleoenvironmental Perspective. AGU Antarctic Research Series, Volume 79.* E. Domack, A. Leventer, A. Burnett, R. Bindschadler, P. Convey and M. Kirby, Eds., American Geophysical Union, 31-42.

Simmonds, I., A. Rafter, T. Cowan, A. B. Watkins and K. Keay, 2005: Large-scale vertical momentum, kinetic energy and moisture fluxes in the Antarctic sea ice region. *Bound.-Layer Meteor.,* (in press).

Watkins, A. B., and I. Simmonds, 1998: Relationships between Antarctic sea-ice concentration, wind stress and temperature temporal variability, and their changes with distance from the coast. *Ann. Glaciol.,* **27,** 409-412.

White, W. B., P. Gloersen and I. Simmonds, 2004: Tropospheric response in the Antarctic Circumpolar Wave along the sea ice edge around Antarctica. *J. Climate,* **17,** 2765-2779.

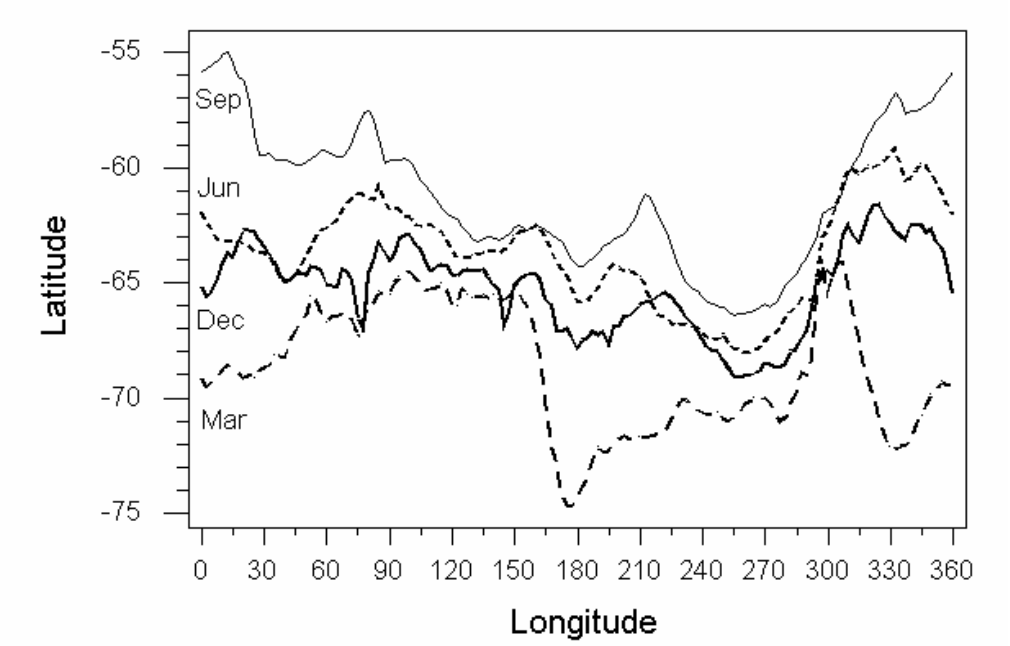

Figure 1: Mean latitude of sea ice edge as a function of longitude for December, March, June and September (1979-2000).

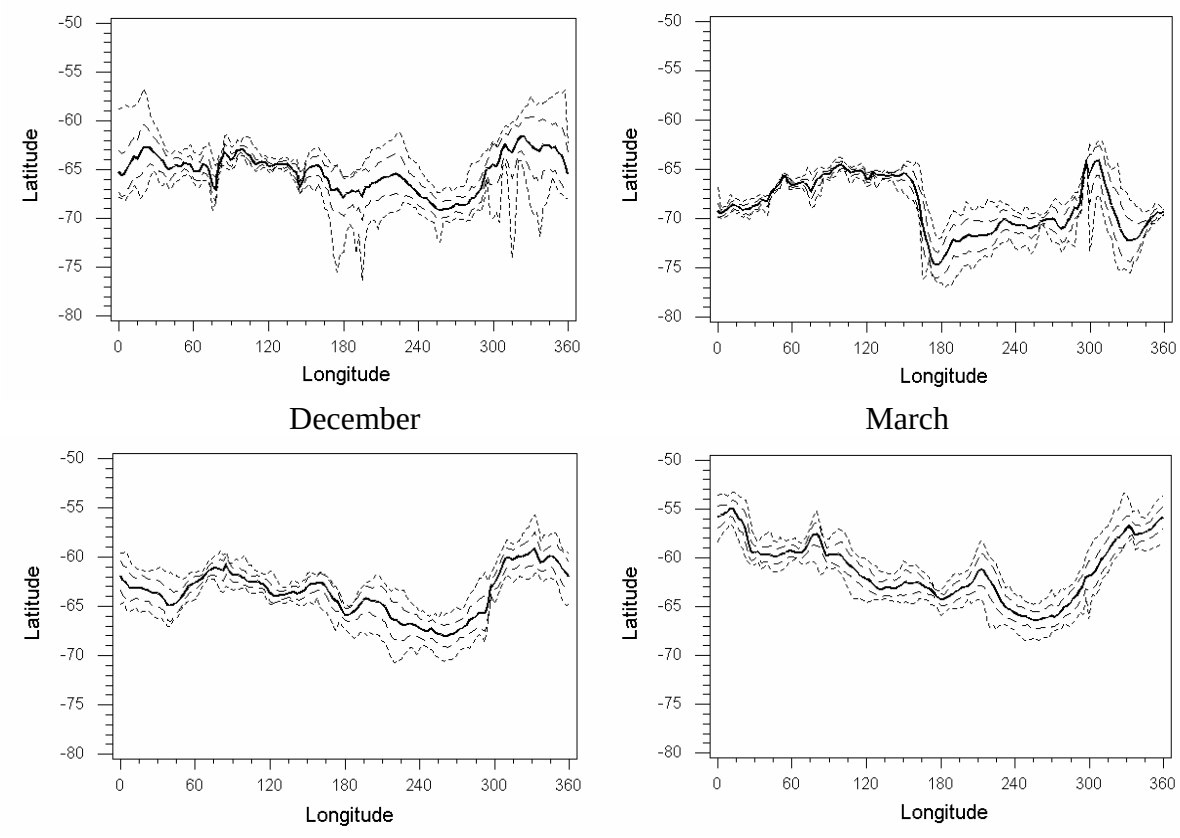

Figure 2: Mean latitude of sea ice edge (bold solid line) with maximum and minimum (short dashed lines) plus the standard deviation of the interannual variations (long dashed lines) in December, March, June and September.

EYE OF THE HURRICANE .

Speranskaya A.A., Anisimova E.P., Moscow, the Moscow State University in the name of M.V. Lomonosov, physical faculty, Lenin mountains, 1/2 2, speransk2004@mail.ru
Pokhil A.E., Russian Hydrometeorological Research Center, 9-11, Big Predtechensky lane, 123242, Moscow, Russia, pokhil@mecom.ru

2004 is marked by a series of powerful tropical cyclones. It may be associated with the global warming. If so, incidence of hurricanes and typhoons will accrue in the future. As a result, there is growing interest to study of TCs.

This article is focused on study of the eye of tropical cyclones (TCs).

Evolution of the eye of tropical cyclones moving on open water areas in the Pacific and the Atlantic was studied at the base of observations from stationary satellites.

Changes of the size of the eye of tropical cyclones were studied depending on pressures in and maximal wind velocities in central cyclone areas. The following trend was identified: a more powerful whirlwind (with lower pressure and greater velocity in the centre) corresponds to a greater radius of the eye. At average, changes of the size of the eye of a whirlwind during TC development are slower, than during TC decline. It was found that at constant (within 60 hour) pressure in TC center, the size of the eye may change in some times.

Causes of fluctuations of diameter of the eye of tropical cyclones can not be identified with use of modern natural observations alone.

The authors sought to fill in this gap, using the results of study of tropical cyclones by laboratory modelling of air intensive convective whirlwinds (ICW) of humid type.

The experimental model - an advanced vortical Fitzjarrald D.E. chamber - provided for the necessary conditions for concentrated whirlwinds such as the background whirlwind and its concentration. In the model a vortex structure emerges, that by the basic criteria of similarity corresponds to the central part of the bottom troposphere of a developed tropical cyclone. The thermal Frud (Fr *) number was found to be the determining criterion of similarity for whirlwinds of such class. The research results obtained with use of ICW physical model at Fr* <0.065 are presented. Under these conditions, there is a clear black "eye" in the center of a whirlwind and, hence, there is no condensed moisture.

In the central area of vortical structure the temperature maximum is observed - the maximum is located at some height from the water surface. While moving away from the axis of a whirlwind, the maximal temperature decreases and moves upwards along the axis of heights. Inversion of temperature in humid ICWs is observed in a thin vertical layer suggesting existence of a local heat source. Measurements of relative humidity in a whirlwind allow to

suggest, that such local heat source is associated with release of condensation heat in the course of phase transition of water.

Presence of a warm nucleus in the central part of a whirlwind results in intensification of density instability in this area. The density instability grows as a result of heat coming from the heated water surface and - particularly - due to release of latent condensation heat.

When density instability reaches some critical size it results in thermal breakdown of the boundary layer that explains explosive nature of vertical heat-and humidity transfer in humid ICWs. The process repeats with some quasi periodical frequency. It should be noted, that increase of density instability in the center of a whirlwind occurs slower than its discharge. It corresponds to observation data when real TCs were observed.

Research studies have shown, that diameter of the eye of a whirlwind also undergoes quasi periodical fluctuations. The function of spectral density of pulsations of diameter of the eye of a whirlwind has a well marked authentic maximum.

The pulsation of diameter of a whirlwind eye can be explained, if we assume, that the stage of increase of the diameter of the eye corresponds to accumulation of density instability in the whirlwind's core, and that its reduction is a result of a break of warm air under "explosive" mechanism of heat and humidity transfer.

Estimates of Struhal numbers describing dimensionless frequency of fluctuations of the diameter of a whirlwind eye, carried out for physical model of intensive convective whirlwind of humid type and for a real tropical cyclone demonstrated a good conformity.

It is possible to assume, that fluctuations of the diameter of the eye of a real TC are of the same nature, as in the model of convective whirlwind. This means that they are associated with the thermal breakdowns peculiar to the explosive mechanism of warm - and humid transfer in the model of humid ICW.

Thus, it is possible to assume, that the explosive mechanism of heat and humidity transfer in a whirlwind similar to TCs identified by physical modelling should be extended to natural intensive convective whirlwinds such as hurricanes and typhoons.

Tracking Tropical Cyclones with Low Level Potential Vorticity

Yury Yusupov
MapMakers Group Ltd., Moscow, Russia, E-mail: usupov@gismeteo.com

The GIS Meteo technology was developed in MapMakers Group Ltd. for use in meteorologist's operational work [1]. In this paper a new tool for tracking tropical cyclones (TC) is represented.

Shapiro and Franklin (1995) documented the potential vorticity (PV) structure of Hurricane Gloria of 1985. They showed that a TC is a strong localized positive PV anomaly in the lower and middle troposphere [2].

PV on isobaric surfaces is calculated using the following equation [3]:

$$PV_p = -g\,[(f + (\partial v/\partial x - \partial u/\partial y)_p)\partial\theta/\partial p + (\partial\theta/\partial y)_p \partial u/\partial p - (\partial\theta/\partial x)_p\,\partial v/\partial p]$$

The appearance of Low Level PV anomaly in Tropics is one of the conditions for the development of TC. Other conditions are: sea surface temperature greater than 26°C, very little vertical shear, relatively high tropospheric moisture, strong disturbance etc.

But the Low Level PV anomaly alone may be used as a precursor of possibile TC development.

The samples (see Fig. 1 and Fig.2 – Atlantic and Pacific regions respectively) are constructed from PV values on isobaric surface at 850 HPa in the grid points where PV is greater than a threshold ($PV_{850} \geq 0.6$ PVU).

The GIS Meteo technology can create forecast charts automatically for arbitrary regions, thus enabling monitoring. You can find daily updated animations of PV_{850} fields in Pacific region on our website in Internet (http://dyn.gismeteo.ru/ANIMOP/typhoon.gif)
As input data we use standard set of GRIB data distributed by WMO.

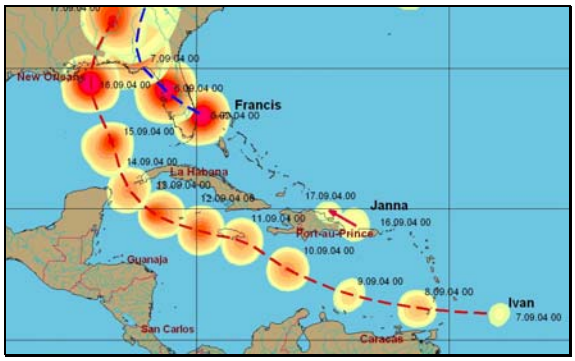

Fig. 1
Hurricanes Francis, Ivan, Janna, September 2004

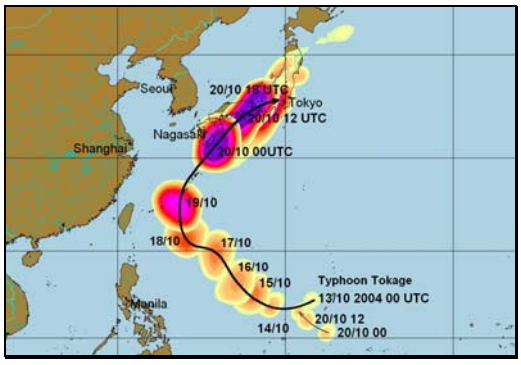

Fig. 2
Typhoon Tokage from 13 of October 2004

References.

1. Akulinicheva A. A., Berkovich L. V., Solomakhov A. I., Shmelkin Y. L., Ioussoupov I. I. The Geographical Information System of Meteo and its usage in meteorological offices in Russia and formed CIS countries. – Meteorology and Hydrology, 2001, N 11, P. 90-98.
2. Shapiro, L.J., Franklin J. L, 1995:Potential Vorticity in Hurricane Gloria. Mon. Wea. Rev., N 123, P. 1465-1475
3. Georgiev C. G. Quantitative relationship between Meteosat WV data and positive potential vorticity anomalies: a case study over the Mediterranean. Meterol. Appl., -1999, N 6, P. 97-109.